Jurnal Teknologi

Full Paper

INFLUENCE OF MACHINING PARAMETERS AND TOOL GEOMETRY ON TOOL WEAR DURING COBALT CHROMIUM-MOLYBDENUM MICRO DRILLING

Mohd Affifudin Abdul Patar[a], Mohd Azlan Suhaimi[a]*, Safian Sharif[a], Amrifan S Mohruni[b], Muhammad Juzaili Hisam[a], Mohd Sallehuddin Shaharum[a]

[a]Faculty of Mechanical Engineering, University Teknologi Malaysia, 81310 UTM Johor Bahru, Johor, Malaysia
[b]Faculty of Mechanical Engineering, Universitas Sriwijaya, 30128, Kota Palembang, Sumatera Selatan, Indonesia

Article history
Received
31 July 2023
Received in revised form
20 September 2023
Accepted
18 October 2023
Published Online
18 February 2024

*Corresponding author
azlansuhaimi@utm.my

Graphical abstract

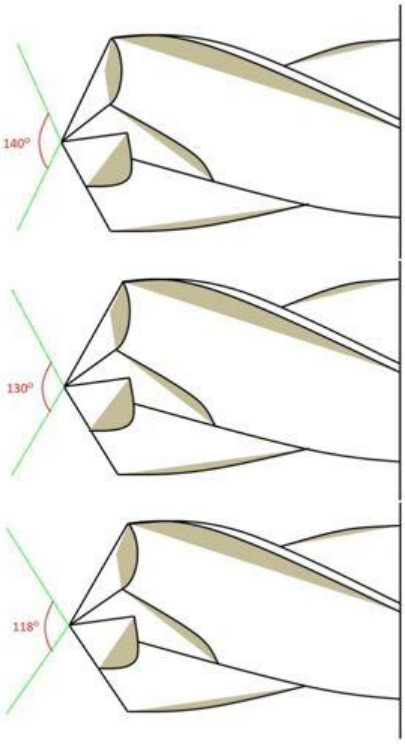

Abstract

Cobalt chromium (CoCr) alloys find extensive use in medical applications due to their unique mechanical properties, such as high strength and low thermal conductivity. However, machining these alloys poses challenges as they are classified as hard-to-cut materials, leading to issues like short tool life, poor surface quality, and low productivity. Rapid tool wear is a significant problem when machining hard alloys, with cutting parameters, drill bit geometry, and types of cutting fluids being the main factors influencing tool wear. In this study, a series of experiments was conducted to investigate the influence of different cutting speeds and tool geometry on tool wear during micro drilling of CoCrMo. A flood cooling system was employed throughout the study, with a constant machining feed rate of 0.1 mm/rev. Three cutting tools with different point angles (118°, 130°, and 140°) and a diameter of 0.2 mm were utilized. The cutting speeds of 50 m/min, 65 m/min, and 80 m/min were varied. A total of 11 runs were performed, with each run consisting of drilling 30 holes. Forces, torques, and tool wear were measured after every subsequent 10 holes drilled. The results indicate that the combination of a 140° point angle and an 80 m/min cutting speed yielded the best performance, exhibiting the lowest force, torque, and tool wear values. The study highlights the importance of selecting appropriate cutting speeds and tool geometry to minimize tool wear and improve machining efficiency when working with CoCr alloys.

Keywords: Tool wear, Tool geometry, Cobalt Chromium Molybdenum, Micro drilling

Abstrak

Aloi kobalt kromium (CoCr) mempunyai kegunaan meluas dalam aplikasi perubatan kerana sifat mekanikalnya yang unik, seperti kekuatan tinggi dan kekonduksian terma yang rendah. Walau bagaimanapun, pemesinan aloi ini menimbulkan cabaran kerana ia diklasifikasikan sebagai bahan yang sukar dipotong, ini membawa kepada isu seperti jangka hayat alat yang pendek, kualiti permukaan yang rapuh dan produktiviti yang rendah. Kadar kehausan alat yang cepat adalah masalah yang ketara apabila pemesinan aloi keras. Antara parameter pemotongan yang penting ialah geometri bit gerudi, dan jenis cecair pemotongan menjadi faktor utama yang mempengaruhi kadar haus alatan. Dalam kajian ini, satu siri eksperimen telah dijalankan untuk menyiasat pengaruh kelajuan pemotongan dan geometri alat yang berbeza terhadap kadar haus alat semasa penggerudian mikro CoCrMo. Sistem

penyejukan banjir telah digunakan sepanjang kajian, dengan kadar suapan pemesinan tetap 0.1 mm/rev. Tiga alat pemotong dengan sudut darjah yang berbeza (118°, 130°, dan 140°) dan diameter 0.2 mm telah digunakan. Kelajuan pemotongan 50 m/min, 65 m/min, dan 80 m/min dipelbagaikan. Sebanyak 11 eksperimen telah dilakukan, dengan setiap experimen terdiri daripada proses menggerudi 30 lubang. Daya, tork, dan kadar haus alatan diukur selepas setiap 10 lubang digerudi. Keputusan menunjukkan bahawa gabungan sudut 140° darjah dan kelajuan pemotongan 80 m/min menghasilkan prestasi terbaik, mempamerkan nilai daya, tork, dan kadar kehausan alat yang paling rendah. Penemuan ini menyumbang kepada pengoptimuman parameter pemesinan untuk penggerudian mikro CoCrMo, memberikan pandangan progresif untuk meningkatkan proses pemesinan bahan yang sukar dipotong dalam aplikasi perubatan. Kajian ini menyerlahkan kepentingan memilih kelajuan pemotongan dan geometri alat yang sesuai untuk meminimumkan kadar kehausan alat dan meningkatkan kecekapan pemesinan aloi CoCr.

Kata kunci: Kadar haus alat, Geometri alat, Kobalt Kromium Molibdenum, Penggerudian mikro

1.0 INTRODUCTION

Superalloy materials, which consist of nickel, cobalt, titanium, or nickel-iron base metal elements, are extensively studied and applied in engineering applications. These materials possess exceptional properties such as high resistance to deformation caused by thermal creep, excellent mechanical strength, good surface stability, and remarkable resistance to corrosion and oxidation. These attributes make superalloys highly suitable for various industrial applications, including aerospace, aircraft turbines, nuclear power systems, biomedical equipment, marine turbine engines, and more [35].

Traditionally, cobalt-chromium alloys are manufactured through casting, and some are forged to achieve the required geometric components to a limited extent. Additionally, machining is often necessary to obtain the desired geometric tolerance and surface finish. Generally, microdrilling is a process which removes material by making holes using minute sized drill bits. Nowadays, micro drilling are applied in various applications such as aircrafts, medical implants, turbines, automotives and cooling holes in jet turbines to name a few[13]. Comparing to other methods of hole production such as lasers and spark machining, micro drilling is prefered as it produces high quality surface finish, geometrical accuracy and lower cost [11].

Micro-drilling and other micro-mechanical machining processes typically employ tools with a diameter of less than 1mm. However, there is variation in the definition of micro drilling among researchers and manufacturers. For instance, Sphinx, a Swiss micro drill manufacturer, defines micro drilling as having a diameter ranging from 0.05 mm to 2.5 mm. On the other hand, Zhuang (2013) defines micro-drill bits as having diameters smaller than 3.175 mm, considering anything larger as no longer falling within the micro-drill category.

High rotational speed combined with a small diameter often leads to common failures in drill tools with diameters less than 1.5 mm, such as breakage. These failures can occur due to excessive thrust force or torque. Consequently, drilling depth and diameter play critical roles in determining the thrust force and torque experienced during drilling. Figure 1 illustrates the geometry of micro-drill bits.

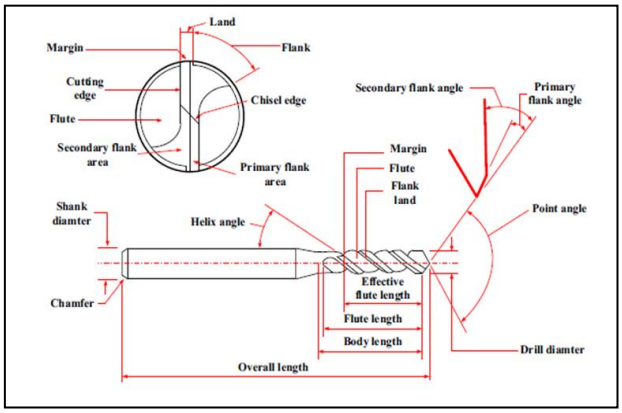

Figure 1 Micro Drill Bit Geometry [13]

In micro-drilling or micro-milling processes, high rotational speed can lead to rapid tool wear, resulting in a deterioration of the machined or drilled surface roughness. As the cutting tool becomes worn, it loses its sharpness, which often leads to the formation of burrs at the drill exit [9]. Previous researchers have investigated the machining of conventional drilling and have achieved positive results by simply changing the tool or using a different coating for the drilling tool [10]. For example,

Benezech *et al*. [4] found out that 130° point angle pairing with 30° rake angle are optimum geometry for chip removal and lower tool wear. Moreover, a study conducted by Zitoune *et al*. [6] found out that drills with diameter 6mm or less are prefered due to the reduction in chisel edge length.

For the purpose of this experiment, a metal alloy consisting of cobalt and chromium, commonly known as cobalt chrome or cobalt chromium, was selected as the material. A CoCrMo block was cut into a thin square bar with dimensions of 60 mm x 60 mm x 4 mm using wire-cutting techniques. The chemical properties of the material are presented in Table 1, while Table 2 provides information on its mechanical properties.

Table 1 Chemical Composition of CoCrMo

Element	Weight (%)
Cr	26-30
Mo	5-7
Fe	0.75
Mn	1.0
Si	1.0
C	0.15-0.35
N	1.0
Ni	0.25
Co	Bal

Table 2 Mechanical Properties of CoCr

Properties	Units	Cobalt Chrome ASTM 1537-Sandvik Value
Proof Stress (0.2%)	MPa	928
Tensile Strength	MPa	1,403
Elongation	%	29
Young's Modulus	GPa	283
Density	$Kg.m^{-3}$	8,768
Thermal Conductivity	$W.m^{-1}.K^{-1}$	14.8
Specific Heat Capacity	$J.Kmg^{-1}.K^{-1}$	452
Thermal Diffusivity	$M^2.s^{-1}$	3.73E-06
Fracture Toughness	$Mpa.m^{1/2}$	100
Hardness	HRC	40

2.0 MATERIALS AND METHODOLOGY

In this study, ASTM F1537 Cobalt Chromium Molybdenum was chosen as the work material. The workpieces had a plate size of 60mm x 60mm x 4mm for length, width, and thickness. Two cutting parameters were considered: cutting speed and different tool geometries. A full factorial design with two levels was employed, resulting in a total of 11 experiments, including 9 factorial experiments and 2 center repetitions. Tools are freshly changed for each runs depending on the parameters selected, each tools only drills 30 holes.

The drilling type used in this experiment was through drilling, and a solid carbide tool bit of the S-type was utilized for the micro-drilling procedure. The S-type tool bit offers specific features and benefits, such as a wider chip pocket, a straight edge profile, a larger K-value, and a corner chamfer edge. The wider chip pocket improves and facilitates chip evacuation, while the straight edge profile produces shorter chips and a reinforced cutting edge. The higher K-value makes the tool suitable for higher feed rates and enhances tool durability. Lastly, the presence of a corner chamfer edge contributes to improved surface finishing [16].

Table 3 Machining Parameters

Factor	Values
Cutting Speed (m/min)	50, 65, 80
Spindle Speed (RPM)	7956, 10350, 12730
Tool Geometry (Point Angle)	118°, 130°, 140°
Feed (mm/rev)	0.1

3.0 MACHINING SETUP

The experiment was conducted using the DMG MORI DMU 50 CNC Machine (Figure 2). Cutting tools used were HPMT custom-made solid carbide twist drills with a diameter of 2mm and varying point angles, as indicated in Table 1. The drilling experiments were performed under flood-cutting conditions, where coolant was continuously applied during the drilling process. Machining parameters are conducted as shown in Table 3.

The outputs of the experiments were tool wear, thrust force, and corresponding torque. Tool wear was observed and measured using the XOPTRON XST150 and XOPTRON X80 Microscopes at different magnifications. The XOPTRON microscope (Figure 2) provided the necessary capabilities for precise measurement and examination of tool wear.

Thrust force was collected using a dynamometer, specifically the Kistler Type 9443B. This dynamometer recorded the cutting force values and data from all coordinates throughout the experiments. It offers excellent rigidity and has a high natural frequency, ensuring accurate force measurements. The

dynamometer's high resolution enables the detection of even the smallest dynamic changes in forces.

Corresponding torque values were calculated based on the collected thrust force data. The combination of the dynamometer and the calculated torque values provided valuable insights into the forces and torques involved in the drilling process.

Figure 2 DMG Mori DMU50 (Top), XOPTRON XST150 Microscope (Bottom)

4.0 RESULTS AND DISCUSSION

A total of 11 experiments were carried out in this study to investigate various aspects of the drilling process. For each experiment, measurements of tool wear, thrust force, and torque were obtained at the 10th, 20th, and 30th holes to track the progression of tool flank wear. The values of thrust force were recorded using the dynamometer, and torque values were calculated based on the force measurements.

All experiments were conducted under the flood cooling method, where coolant was continuously applied during the drilling process to control temperature and improve lubrication.

The collected data, specifically the values of thrust force, are presented in Table 4, which provides an overview of the force measurements obtained for all 11 experiments conducted in the study.

The observed trend in Table 4 indicates that the lowest force occurred when the cutting speed was highest at 80 m/min with a 140° point angle drill bit. Conversely, the highest force was observed when the lowest cutting speed of 50 m/min was paired with a 118° point angle drill bit. This relationship can be explained by the effect of temperature on the material during the machining process. As the temperature increases, the material softens, leading to a decrease in its hardness. Consequently, less force is required for the machining process. This explanation is supported by the findings of Dang *et al*. (2019), who stated that an increase in spindle speed results in a rapid rise in cutting temperature, leading to a stronger thermal softening effect on the material. With a softer material, the thrust force decreases significantly.

Additionally, increasing the spindle speed reduces the contact time between the material and the tool, thereby reducing the plastic deformation of the material. This finding is consistent with the results reported by Venkatesen *et al*. (2020) in their study on micro-drilling Inconel 800. The relationship between cutting speed, tool geometry, and the corresponding force and torque output can be better visualized in the graphs provided below. Figure 3 and 4 below shows the relationship between cutting speed (m/min) against force and its corresponding torque for all three different tool geometries.

Table 4 Average Force Output for CoCrMo Bulk Material

Run	Hole No	Speed (m/min)	Tool	Forces (N)			Force Average	Run Avg Force (N)
				1	2	3		
1	10	50	Tool A (140°)	189.20	188.29	187.42	188.31	189.63
	20	50		187.44	187.26	186.94	187.22	
	30	50		193.51	193.46	193.13	193.37	
2	10	65		161.91	161.88	160.82	166.36	170.55
	20	65		169.79	169.10	168.19	169.03	
	30	65		176.86	176.21	175.70	176.26	
3	10	80		166.33	165.71	165.20	165.75	167.38
	20	80		162.56	162.28	162.05	162.29	
	30	80		174.76	173.80	173.72	174.10	
4	10	50	Tool B (130°)	200.07	198.44	198.30	198.94	199.72
	20	50		198.24	198.00	197.96	198.07	
	30	50		202.81	201.951	201.66	202.14	
5	10	65		171.33	171.12	170.88	171.11	185.5
	20	65		177.45	175.00	174.71	175.72	
	30	65		210.88	209.18	208.94	209.67	
6	10	80		215.60	213.78	212.90	214.09	226.09
	20	80		225.82	224.19	223.67	224.56	
	30	80		241.02	239.29	238.58	239.63	
7	10	50	Tool C (118°)	1042.01	1041.14	1039.71	1040.95	1113.62
	20	50		1189.82	1184.85	1184.19	1186.29	
8	10	65		532.83	531.88	531.83	532.18	626.25
	20	65		721.55	720.00	719.40	720.32	
9	10	80		634.07	630.83	631.66	632.52	632.52
10 (rep)	10	65	Tool B (130°)	203.94	202.50	202.47	202.96	204.71
	20	65		200.46	199.57	199.22	199.75	
	30	65		211.76	211.32	211.15	211.41	
11 (rep)	10	65		203.31	203.18	203.17	203.22	206.29
	20	65		203.41	203.16	203.02	203.20	
	30	65		213.54	212.21	211.60	212.45	

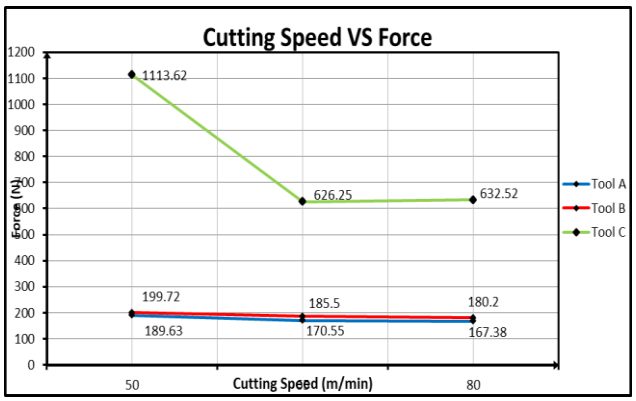

Figure 3 Cutting Speed VS Force Graph for Different Type of Tool

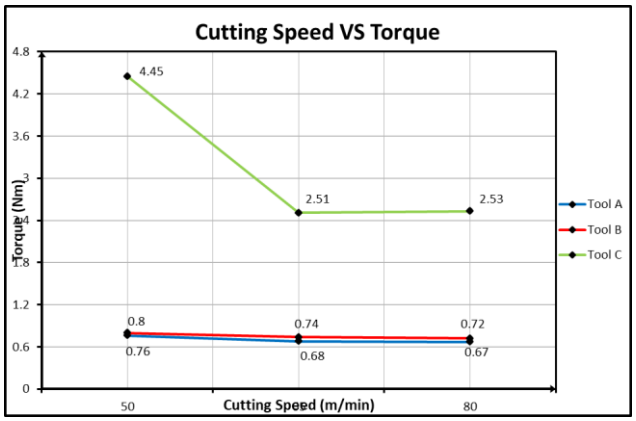

Figure 4 Cutting speed vs torque graph for different types of tool

The graph presented in Figure 3 illustrates an inverse relationship between cutting speed and thrust force, indicating that as the cutting speed increases, the forces decrease. Similarly, Figure 4 demonstrates the inverse relationship between cutting speed and the corresponding torque. This relationship holds true for all three different tool geometries. Among the three tool geometries, Tool C, with a point angle of 118°, exhibits the highest force and torque outputs, while Tool A, with a point angle of 140°, shows the lowest values for forces and torques. The graphs also reveal a relationship between tool geometry, output force, and corresponding torque at three different instances of cutting speed. The point angle values of the tools are inversely proportional to the force and torque values. A smaller point angle results in longer cutting edges and a smaller contact area between the cutting edge and the material. This leads to a more concentrated distribution of force and higher force and torque values, as supported by Hassan *et al.* (2018) in their study on drilling composite metals.

In this experiment, cutting fluids were used during the machining process, employing the flood cooling method to facilitate efficient chip removal. Micro drill bits have small cavities, and the chips can easily become jammed, potentially increasing the machining temperature. The temperature elevation can impact the cutting capability of the tool and influence tool wear rates [5]. The flood cooling method adopted in this study serves to enhance tool life, particularly for micro-sized drill bits. Table 5 presents the average wear rate of each tool under different machining speeds and tool point angles while maintaining a constant feed rate and cooling method.

In this experiment, the tool life criterion is based on the ISO 8688-2 standard. According to this criterion, the limit for tool wear in micro drill bits is set at 0.3mm. Any wear value exceeding this limit is considered a failure. The flank wear of the micro drill bits is specifically taken into consideration. Due to limited material resources, the wear values of the drill bits are measured after every 10 holes drilled, up to the 30th hole. Table 5 reveals that the highest wear rate of the tool bit is observed when the cutting speed is 50 m/min and Tool C, which has a point angle of 118°, is employed. Conversely, the lowest wear rate is observed when the cutting speed is at its maximum of 80 m/min, and Tool A, with a point angle of 140°, is used.

The point angle of the drill bit influences its sharpness, which in turn affects the output of thrust force and torque. On the other hand, cutting speed influences the cutting-edge radius in the micro-drilling process [14]. The results obtained in Table 5 support the observation that increasing the point angle value leads to a decrease in thrust force, as described above. Another study conducted by Venkatesan *et al.* (2020) has demonstrated that as the cutting speed increases, the cutting-edge radius also increases. This increase in cutting-edge radius negatively impacts dimensional accuracy and leads to excessive wear. The table further confirms that as the speed increases, the wear of the drill bits also increases.

Table 6 presented below illustrates the wear progression of each Tool A from the 10th hole to the 20th hole and finally, the 30th hole. The tool geometry and feed rate were kept constant with a point angle of 140° and a feed rate of 0.1 mm/rev. However, the cutting speed varied across the experiments, with values of 50 m/min, 65 m/min, and 80 m/min.

Table 7 presented below depicts the wear progression of each Tool B from the 10th hole to the 20th hole and, finally, the 30th hole. Throughout these experiments, the tool geometry and feed rate were kept constant, with a point angle of 130° and a feed rate of 0.1 mm/rev. However, the machining cutting speed varied among the experiments, ranging from 50 m/min to 80 m/min.

Table 5 Average Wear of Tool

Run	Hole No	Speed (m/min)	Tool	Avg Wear
1	10	50	Tool A (140°)	0.100
	20	50		
	30	50		
2	10	65		0.117
	20	65		
	30	65		
3	10	80		0.105
	20	80		
	30	80		
4	10	50	Tool B (130°)	0.12
	20	50		
	30	50		
5	10	65		0.141
	20	65		
	30	65		
6	10	80		0.155
	20	80		
	30	80		
7	10	50	Tool C (118°)	0.36
	20	50		
8	10	65		0.326
	20	65		
9	10	80		0.305
10 (rep)	10	65	Tool B (130°)	0.12
	20	65		
	30	65		
11 (rep)	10	65		0.123
	20	65		
	30	65		

Table 6 Wear Progression for Tool-A Drill Bit (140°)

Tool A	50 m/min	65 m/min	80 m/min
10th Hole	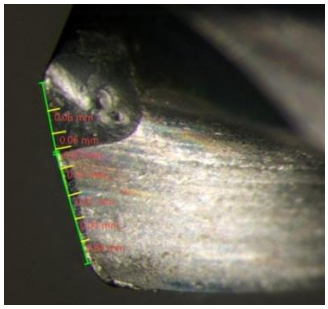	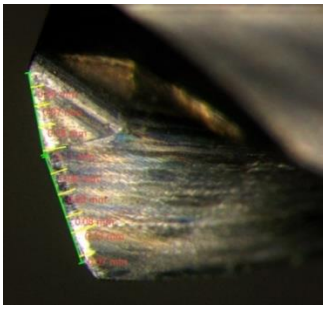	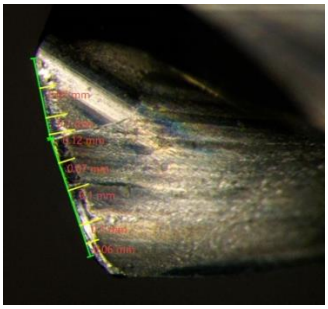
20th Hole	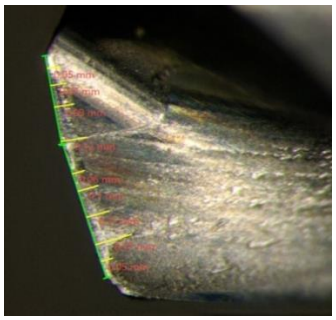	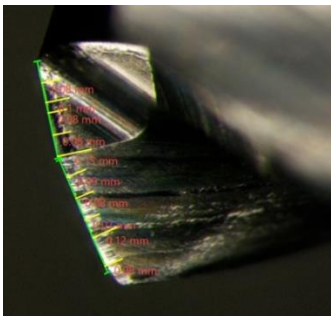	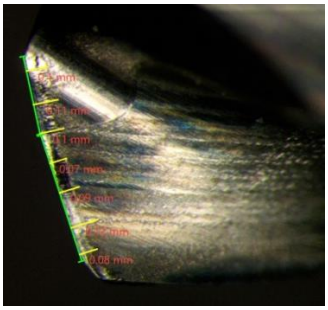
30th Hole	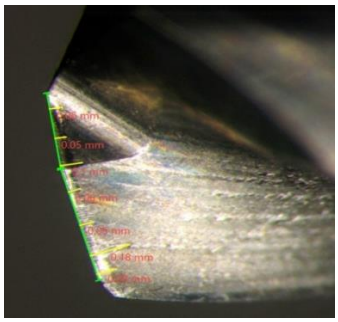	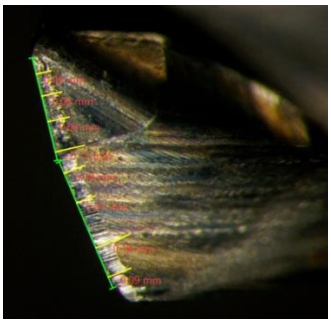	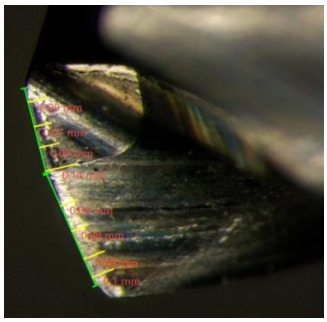

Table 7 Wear Progression for Tool-B Drill Bit (130°)

Tool B	50 m/min	65 m/min	80 m/min
10th Hole	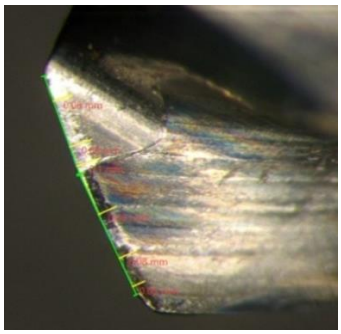	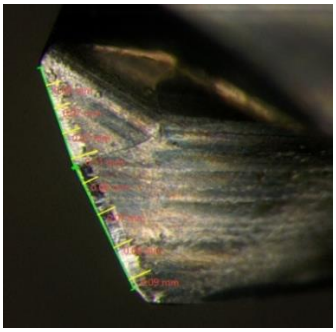	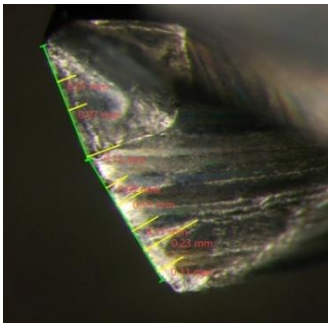
20th Hole	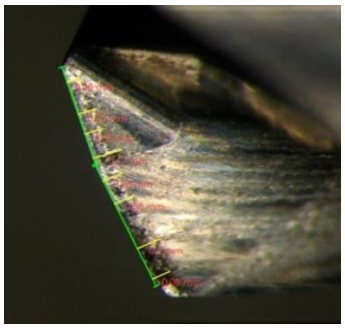	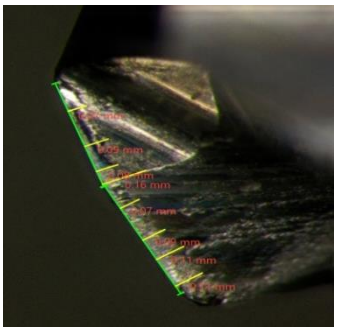	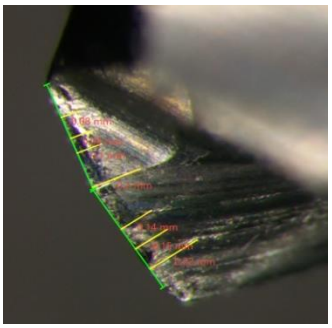
30th Hole	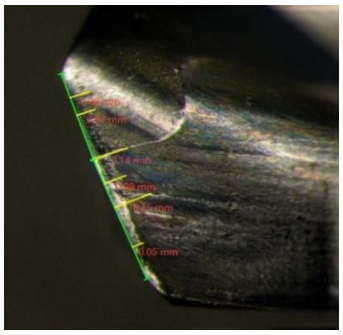	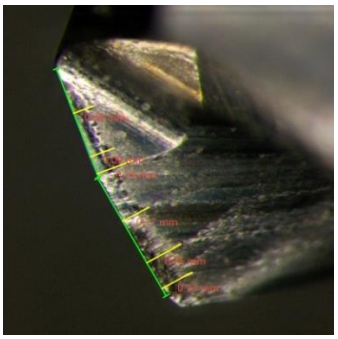	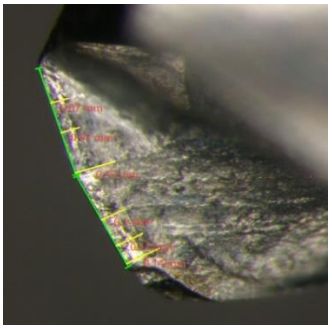

Table 8 Wear Progression for Tool-C Drill Bit (118°)

Tool C	50 m/min	65 m/min	80 m/min
10th Hole	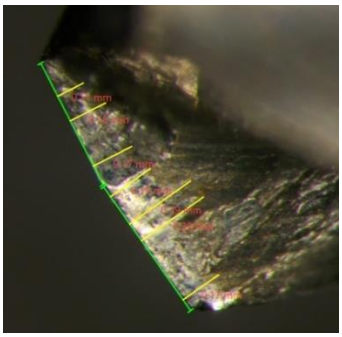	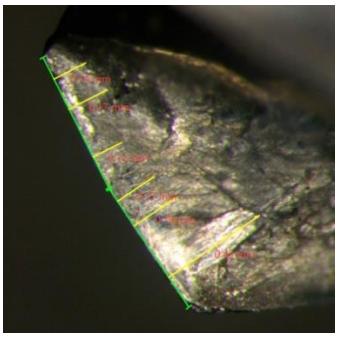	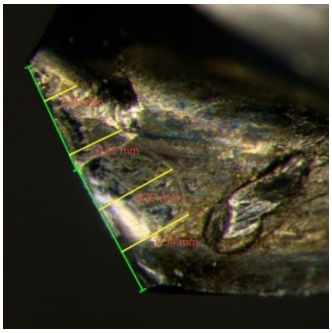
20th Hole	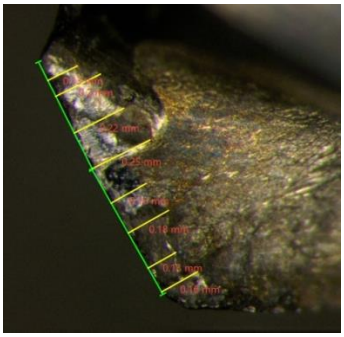	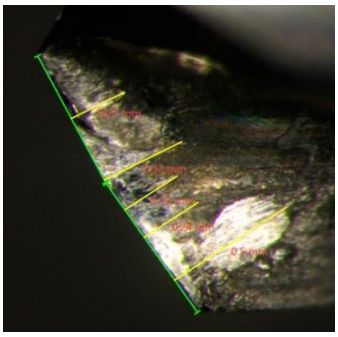	

Table 8 presented above, displays the wear progression of each Tool C. For the experiments conducted at 50 m/min and 65 m/min, the wear measurements were recorded up to the 20th hole. However, for the experiment conducted at 80 m/min, the wear measurements were only recorded up to the 10th hole. This limitation is due to the achievement of the tool life criterion for wear. Throughout these experiments, the tool geometry and feed rate were maintained constant, with a point angle of 118° and a feed rate of 0.1 mm/rev. The machining cutting speed varied among the experiments, ranging from 50 m/min to 80 m/min.

To summarize and demonstrate the relationship between tool geometries, cutting speed, and tool wear, the graph in Figure 5 is presented. Tool A, Tool B, and Tool C have point angles of 140°, 130°, and 118°, respectively. The graph illustrates the relationship between tool geometries and average wear at three different machining speeds. The trend depicted in Figure 5 remains consistent across all three speeds. The relationship between tool geometry and average wear is inversely proportional. As the point angle of the tool decreases, the average wear at a given machining speed increases. This observation is supported by the findings of Jadhav *et al*. (2018) in their study on drilling AL6061, where they noted that reducing the point angle leads to higher machining forces and torques, ultimately accelerating tool wear.

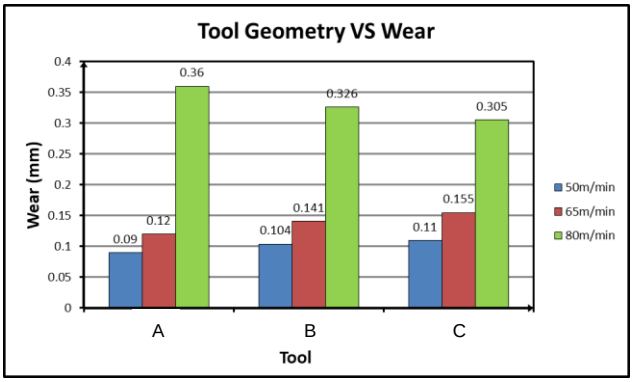

Figure 5 Tool geometry vs. wear graph for increasing machining speed

Figure 6, presented below, illustrates the relationship between cutting speed and tool wear for three different tool geometries. Tools 1 and 2 exhibit a similar trend, where tool wear is directly proportional to cutting speed. However, for Tool C, the relationship is inverse, indicating that tool wear decreases as the machining speed increases. It is worth noting that while the wear progression rate of

Tool C shows a positive trend with increased cutting speed, all the tool wear values for Tool C exceeded the tool life criterion for failure. This suggests that the geometry of Tool C is not suitable for this particular study. This observation aligns with the findings of Dang *et al*. (2019), who conducted a similar study and demonstrated that increased cutting speed results in higher drilling forces, leading to an elevated wear rate and subsequent rise in cutting temperature. The increased temperatures primarily result from the friction between the machined surface and the flank face of the tool.'

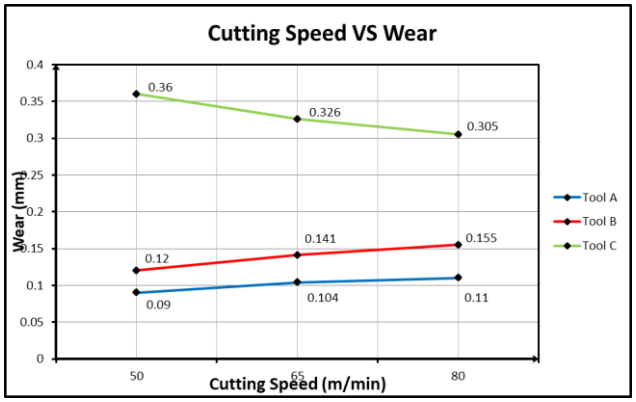

Figure 6 Cutting Speed VS Wear Graph for Different Tool Geometry

4.1 Response Surface Methodology (RSM)

RSM is a basic collection of mathematical and statistical method which is utilized for modeling and analyzing problems in which the response of interest were influenced by several variables. This method then depicts the relationship between one or more measured response and finally it could optimize it. This technique is used in this study to further analyze all the results obtained earlier, output responses is tabulated in the ANOVA (Table 9 and 10).

"Prob>F" value is shown to be less than 0.05, this output allow this study to conclude that the regression model tabulated is significant and the variables in the model obtained significantly affect the response. Following the obtained results from this study, all of the variables and parameters show notable impact on the model for the cutting force response. This is evidently shown by the insignificant lack-of-fit, having high value of R^2 closing to 1. As for the wear ANOVA table, it is also shown that the main effect of tool geometry (point angle) were the significant model terms. Through the observation obtained from experimental works, as the point angle is decrease the wear gradually increases. A smaller point angle results in longer cutting edges and a smaller contact area between the cutting edge and the material. This leads to a more concentrated distribution of force and higher force and torque values. The following equations are the final empirical models in terms of coded which obtained from optimized parameters:
Thrust Force:

$$F\ (N) = 137.11 - 90.72A - 307.47B + 98.05A^2 + 280.85B^2 + 117.91AB$$

Wear:

$$Wear\ (mm) = 0.095 - 2.891E\text{-}0.03A - 0.11B + 0.029A^2 + 0.10B^2 + 0.016AB$$

Where;
A = Cutting Speed
B = Point Angle

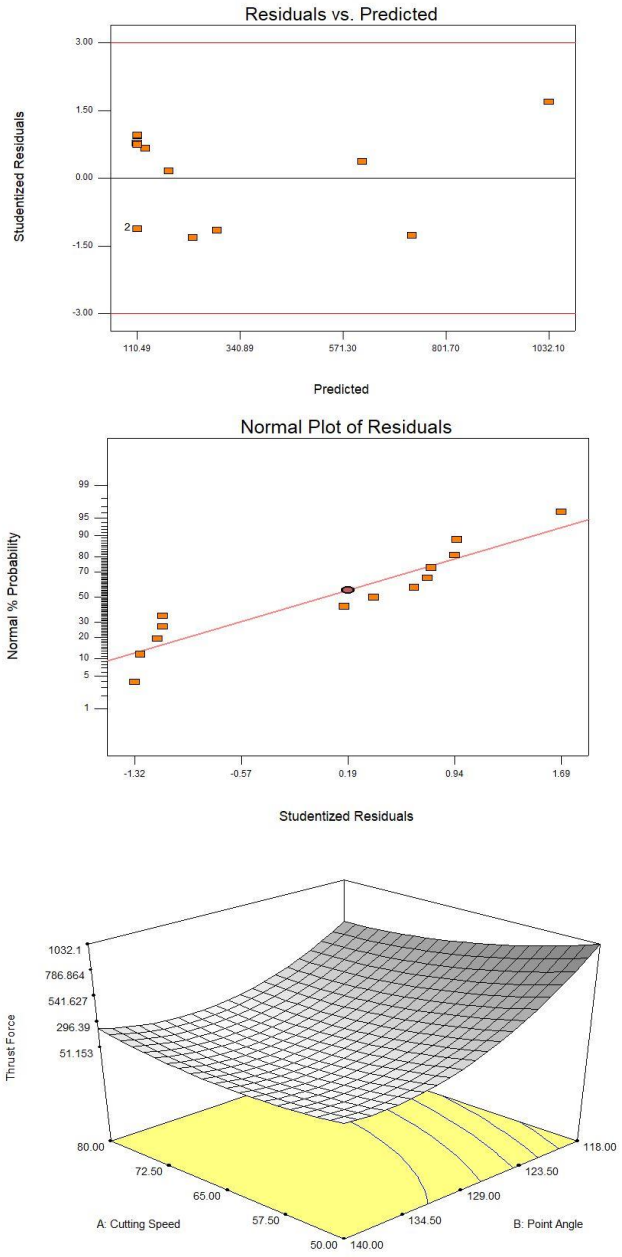

Figure 7 Diagnostics and Model Graphs for Thrust Force

Table 9 ANOVA table (partial sum of squares) for response quadratic model (response: thrust force)

Source	Sum of Squares	DF	Mean Square	F Value	Prob > F	
Model	1.077E+006	5	2.154E+005	18.00	0.0007	*Significant*
A	49310.67	1	49310.67	4.12	0.0820	
B	5.672E+005	1	5.672E+005	47.39	0.0002	
A	26550.07	1	26550.07	2.22	0.1800	
B	2.135E+005	1	2.135E+005	17.83	0.0039	
AB	55759.72	1	55759.72	4.66	0.0678	
Residual	83789.12	7	11969.87			
Lack of Fit	36079.57	3	12026.52	1.01	0.4761	*Not significant*
Pure Error	47709.55	4	11927.39			
Cor Total	1.161E+006	12				

Table 10 ANOVA table (partial sum of squares) for response quadratic model (response: wear)

Source	Sum of Squares	DF	Mean Square	F Value	Prob > F	
Model	0.13	5	0.026	7.47	0.0100	*Significant*
A	5.324E-005	1	5.324E-005	0.015	0.9044	
B	0.075	1	0.075	21.72	0.0023	
A	2.398E-003	1	2.39E-003	0.70	0.4310	
B	0.029	1	0.029	8.55	0.0222	
AB	1.010E-003	1	1.010E-003			
Residual	0.024	7	3.435E-003			
Lack of Fit	4.124E-003	3	1.375E-003	0.28	0.8407	*Not significant*
Pure Error	0.15	12				
Cor Total						

Figure 7 and 8 shows the normal probability graph which displays normally distributed errors that typically fall along the straight line. There is no noticeable pattern or out of norm structure observed in both residuals versus predicted response data. This shows that the proposed models are sufficient and that neither the assumption of independence nor the assumption of constant variance has been breached. The curvilinear profile of the 3D models successfully captures the relationship between factors and responses.

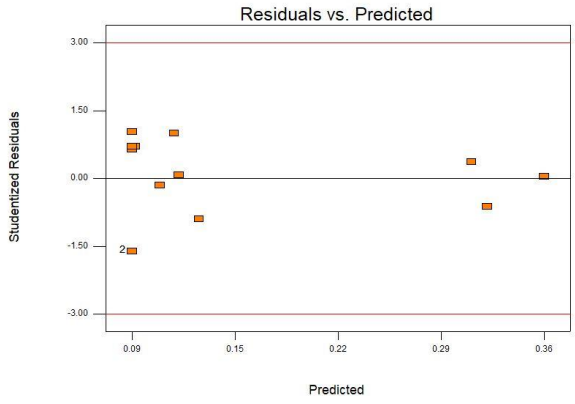

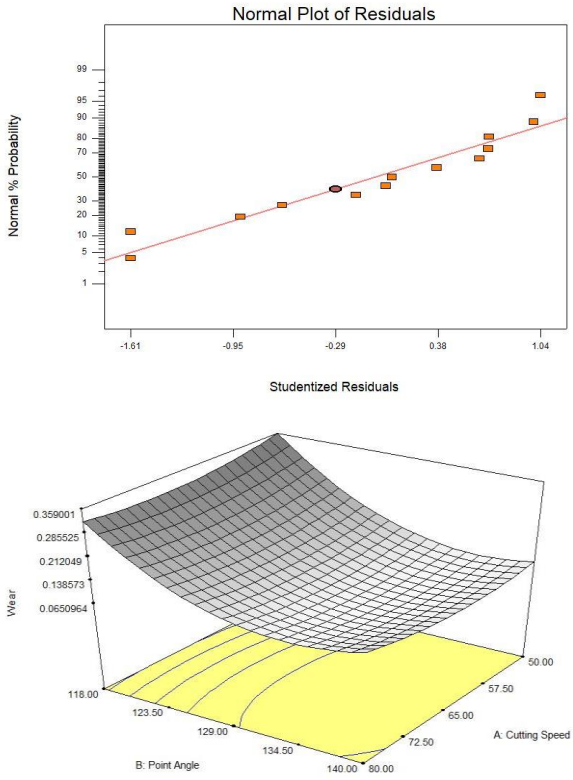

Figure 8 Diagnostics and Model Graphs for Wear

5.0 CONCLUSION

This paper investigates the impact of different tool geometries and machining speeds on tool wear during the micro drilling of CoCrMo bulk material. The results highlight the variations in force, torque, and tool wear based on the combinations of parameters. Tool geometry was modified by altering the point angles, while three different cutting speeds were utilized. The findings reveal that the optimal output was achieved with Tool A, which had a point angle of 140°, paired with the highest cutting speed of 80 m/min. This combination yielded the lowest average force of 167.38N and torque of 0.67Nm. Furthermore, the tool wear after drilling 30 holes was the lowest, with an average wear of only 0.105mm. Conversely, the least favorable results were obtained with Tool C, which had a point angle of 118° and a cutting speed of 50 m/min. This combination resulted in the highest average force of 1,113.63N and torque of 4.45Nm. Additionally, the average wear of the tool after the run was the highest, exceeding the tool life criterion limit of 0.30mm, with an average wear of 0.36mm. Consequently, Tool C is not well-suited for the micro-drilling of CoCrMo.

Conflicts of Interest

The author(s) declare(s) that there is no conflict of interest regarding the publication of this paper.

Acknowledgement

The author gratefully acknowledges the financial support from Universiti Teknologi Malaysia under UTM High Impact Grant (HIR) with grant No: Q.J130000.2409.08G37 and Q.J130000.4351.09G66.

References

[1] Aerospace Materials: Past, Present and Future. 2012. *Introduction to Aerospace Materials*. Elsevier. 15-38.
[2] Agarwala, David Bourell, Joseph Beaman, Harris Marcus, M. *et al.* 1995. Introduction Direct Selective Laser Sintering of Metals. *Rapid Prototyping Journal*. 1: 26-36.
[3] Akhavan Farid, A., Sharif, S. and Idris, M. H. 2011. Chip Morphology Study in High Speed Drilling of Al-Si Alloy. *International Journal of Advanced Manufacturing Technology*. 57(5-8): 555-564.
[4] Benezech, L., Landon, Y., & Rubio, W. 2012. Study of Manufacturing Defects and Tool Geometry Optimisation for Multi-material Stack Drilling. *Advanced Materials Research*. 423: 1-11.
[5] Perçin, M., Aslantas, K., Ucun, I., Kaynak, Y., & Çicek, A. 2016. Micro-drilling of Ti-6Al-4V Alloy: The Effects of Cooling/lubricating. *Precision Engineering*. 45: 450-462.
[6] Zitoune, R., Krishnaraj, V., & Collombet, F. 2010. Study of Drilling of Composite Material and Aluminium Stack. *Composite Structures*. 92(5): 1246-1255.
[7] Baron, S., Desmond, D. and Ahearne, E. 2019. The Fundamental Mechanisms of Wear of Cemented Carbide in Continuous Cutting of Medical Grade Cobalt Chromium Alloy (ASTM F75). *Wear*. 424-425: 89-96.
[8] Breitling, D. *et al.* (no date) Drilling of Metals. Çakir Şencan, A., Duran, A. and Şeker, U. 2020 The Effect of Different Cooling Methods to Hole Quality and Tool Life in the Drilling of AA7075 and AA2024 Aluminum Alloys.
[9] Dornfeld, D., Min, S. and Takeuchi, Y. 2006. Recent Advances in Mechanical Micromachining. *CIRP Annals - Manufacturing Technology*. 55(2): 745-768.
[10] Hassan, M. H., Abdullah, J., Mahmud, A. S., & Supran, A. 2018. Effect of Drill Geometry and Drilling Parameters on the Formation of Adhesion Layer in Drilling Composite-metal Stack-up Material. *Journal of Mechanical Engineering*. 5(Special Issue 2): 90-98.
[11] Widodo, Redzuan, N., & Kurniawan, D. 2015. Evaluation of Hole Quality on Microdrilling AISI304 Austenitic Stainless Steel. *Procedia Manufacturing*. 2(February): 465-469.
[12] Harun, M. H. S., Ghazali, M. F. and Yusoff, A. R. 2017. Analysis of Triaxial Force and Vibration Sensors for Detection of Failure Criterion in Deep Twist Drilling Process. *International Journal of Advanced Manufacturing Technology*. 89(9-12): 3535-3545.
[13] Hasan, M., Zhao, J. and Jiang, Z. 2017. A Review of Modern Advancements in Micro Drilling Techniques. *Journal of Manufacturing Processes*. Elsevier Ltd. 343-375.
[14] Hegab, H. and Kishawy, H. 2018. Towards Sustainable Machining of Inconel 718 Using Nano-Fluid Minimum Quantity Lubrication. *Journal of Manufacturing and Materials Processing*. 2(3): 50.
[15] Hu, P. S. *et al.* 2014. Investigation of Wear and Corrosion of a High-carbon Stellite Alloy for Hip Implants. *Journal of Materials Engineering and Performance*. 23(4): 1223-1230.
[16] High Precision Machining Tool (HPMT). General Catalogue E, Solid Carbide Tools.
[17] Jain, A. and Bajpai, V. 2020. Introduction to High-speed Machining (HSM). *High-Speed Machining*. Elsevier. 1-25.
[18] Keaveney, S. *et al.* 2015. An Assessment of Medical Grade Cobalt Chromium Alloy ASTM F1537 as a Difficult-to-Cut (DTC) Material an Assessment of Medical Grade Cobalt Chromium Alloy ASTM F1537 as a 'Difficult-to-Cut (DTC)' Material.
[19] Khanafer, K. *et al.* 2020. Toward Sustainable Micro-drilling of Inconel 718 Superalloy using MQL-Nanofluid. *International Journal of Advanced Manufacturing Technology*. 107(7-8): 3459-3469.
[20] Kishawy, H. A. *et al.* 2005. Effect of Coolant Strategy on Tool Performance, Chip Morphology and Surface Quality during High-speed Machining of A356 Aluminum Alloy. *International Journal of Machine Tools and Manufacture*. 45(2): 219-227.
[21] Kiswanto, G., Zariatin, D. L. and Ko, T. J. 2014. The Effect of Spindle Speed, Feed-rate and Machining Time to the Surface Roughness and Burr Formation of Aluminum Alloy 1100 in Micro-milling Operation. *Journal of Manufacturing Processes*. 6(4): 435-450.
[22] Jiaqiang Dang, Gongyu Liu, Yaofeng Chen, Qinglong An, Weiwei Ming & Ming Chen. 2019. Experimental investigation on machinability of DMLS Ti6Al4V under dry drilling process. *Materials and Manufacturing Processes*. 34(7): 749-758.
[23] Jadhav, S. S., Kakde, A. S., Patil, N. G., & Sankpal, J. B. 2018. Effect of Cutting Parameters, Point Angle and Reinforcement Percentage on Surface Finish, in Drilling of AL6061/Al2O3p MMC. *Procedia Manufacturing*. 20: 2-11.
[24] Schweiger, J. *et al.* 2020. Internal Porosities, Retentive Force, and Survival of Cobalt–chromium Alloy Clasps Fabricated by Selective Laser-sintering. *Journal of Prosthodontic Research*. 64(2): 210-216.
[25] Vaicelyte, A. *et al.* 2020. Cobalt–chromium Dental Alloys: Metal Exposures, Toxicological Risks, CMR Classification, and EU Regulatory Framework. *Crystals*. 1–16.
[26] Aamir, M., Tu, S., Giasin, K., & Tolouei-Rad, M. 2020. Multi-hole Simultaneous Drilling of Aluminium Alloy: A Preliminary Study and Evaluation against One-shot Drilling Process.

Journal of Materials Research and Technology. 9(3): 3994-4006.
[27] Barman, A., Adhikari, R., & Bolar, G. 2020. Evaluation of Conventional Drilling and Helical Milling for Processing of Holes in Titanium Alloy Ti6Al4V. *Materials Today: Proceedings*. 28: 2295-2300.
[28] Bogajo, I. R., Tangpronprasert, P., Virulsri, C., Keeratihattayakorn, S., & Arrazola, P. J. 2020. A Novel Indirect Cryogenic Cooling System for Improving Surface Finish and Reducing Cutting Forces when Turning ASTM F-1537 Cobalt-chromium Alloys. *International Journal of Advanced Manufacturing Technology*. 111(7-8): 1971-1989.
[29] Venkatesan, K., Nagendra, K. U., Anudeep, C. M., & Cotton, A. E. 2021. Experimental Investigation and Parametric Optimization on Hole Quality Assessment During Micro-drilling of Inconel 625 Superalloy. *Arabian Journal for Science and Engineering*. 46(3): 2283-2309.
[30] Haja Syeddu Masooth, P., & Jayakumar, V. 2020. Experimental Investigation on Surface Finish of Drilled Hole by TiAlN, TiN, AlCrN coated HSS Drill under Dry Conditions. *Materials Today: Proceedings*. 22: 315-321.
[31] Khanna, N., Zadafiya, K., Patel, T., Kaynak, Y., Rahman Rashid, R. A., & Vafadar, A. 2021. Review on Machining of Additively Manufactured Nickel and Titanium Alloys. *Journal of Materials Research and Technology*. 15: 3192-3221.
[32] Suresh Kumar, B., Baskar, N., & Rajaguru, K. 2020. Drilling Operation: A Review. *Materials Today: Proceedings*. 21: 926-933.
[33] Zhao, S. *et al*. 2003. Microstructural Stability and Mechanical Properties of a New Nickel-based Superalloy. *Materials Science and Engineering A*. 355(1-2): 96-105.